



Ag-modified hydrogen titanate nanowire arrays for stable lithium metal anode in a carbonate-based electrolyte

Zhipeng Wen^a, Dongzheng Wu^a, Hang Li^a, Yingxin Lin^b, Hang Li^b, Yang Yang^{c,*}, Jinbao Zhao^{a,*}

^aState Key Lab of Physical Chemistry of Solid Surfaces, Collaborative Innovation Centre of Chemistry for Energy Materials, State-Province Joint Engineering Laboratory of Power Source Technology for New Energy Vehicle, Engineering Research Center of Electrochemical Technology, Ministry of Education, College of Chemistry and Chemical Engineering, Xiamen University, Xiamen 361005, Fujian, China

^bCollege of Energy & School of Energy Research, Xiamen University, Xiamen 361102, Fujian, China

^cSchool of Chemical Engineering and Light Industry, Guangdong University of Technology, Guangzhou 510006, Guangdong, China

ARTICLE INFO

Article history:

Received 6 May 2020

Revised 18 May 2020

Accepted 25 May 2020

Available online 5 June 2020

Keywords:

Hydrogen titanate nanowire arrays

Ag nanoparticles

Li metal anode

Carbonate-based electrolyte

ABSTRACT

In the investigation of the next-generation battery anode, Li metal has attracted increasing attention owing to its ultrahigh specific capacity and low reduction potential. However, its low coulombic efficiency, limited cycling life, and serious safety hazards have hindered the practical application of rechargeable Li metal batteries. Although several strategies have been proposed to enhance the electrochemical performance of Li metal anodes, most are centered around ether-based electrolytes, which are volatile and do not provide a sufficiently large voltage window. Therefore, we aimed to attain stable Li deposition/stripping in a commercial carbonate-based electrolyte. Herein, we have successfully synthesized hydrogen titanate (HTO) nanowire arrays decorated with homogenous Ag nanoparticles (NPs) (Ag@HTO) via simple hydrothermal and silver mirror reactions. The 3D cross-linked array structure with Ag NPs provides preferable nucleation sites for uniform Li deposition, and most importantly, when assembled with the commercial $\text{LiNi}_{0.5}\text{Co}_{0.2}\text{Mn}_{0.3}\text{O}_2$ cathode material, the Ag@HTO could maintain a capacity retention ratio of 81.2% at 1 C after 200 cycles, however the pristine Ti foil failed to do so after only 60 cycles. Our research therefore reveals a new way of designing current collectors paired with commercial high voltage cathodes that can create high energy density Li metal batteries.

© 2020 Science Press and Dalian Institute of Chemical Physics, Chinese Academy of Sciences. Published by ELSEVIER B.V. and Science Press. All rights reserved.

1. Introduction

In 2019, the Nobel Prize in Chemistry was awarded jointly to John B. Goodenough, M. Stanley Whittingham, and Akira Yoshino for their outstanding contributions to lithium-ion batteries (LIBs) under the topic “for the development of lithium-ion batteries”. Since the launch of the commercial LIBs in the mobile electronics market by the SONY Corporation in the early 1990s, vast and dramatic effects have been witnessed in the way society has benefited from LIBs [1]. An anode is an indispensable component in a LIB and is comprised of graphite. With the continuous advancement in technology, graphite anode materials have approached their maximum theoretical capacity limit (372 mAh g^{-1}) [2]. However, the demand for high energy density batteries in large-scale energy storage systems continues to expand. This burgeoning

gap between technology advancements and market demand has led to numerous challenges [3]. Furthermore, Li metal has recently garnered considerable attention as a potential anode candidate owing to its ultrahigh gravimetric specific capacity (3860 mAh g^{-1}) and low reduction potential (-3.04 V compared with a standard hydrogen electrode). Moreover, this metal also meets the requirements of the new-generation positive electrodes, such as sulfur and oxygen, which greatly improve the overall energy density of batteries. In this regard, the development of a high-performance Li metal anode has the potential to revolutionize the entire energy storage consumer market [4–6].

Unfortunately, the poor coulombic efficiency and limited cycling lifespan seriously hinder the practical commercialization of Li metal anodes. The unstable electrolyte/electrode interface and the formation of Li dendrites are among the primary issues. Highly reactive Li metal easily reacts with electrolytes to form a solid electrolyte interface (SEI) on the surface [7,8]. Theoretically, during the Li deposition process, the volume expansion ratio tends to be infinite in the absence of a deposition host. However, a

* Corresponding authors.

E-mail addresses: yangyang@gdut.edu.cn (Y. Yang), jbzha@xmu.edu.cn (J. Zhao).

traditionally generated SEI is not flexible enough and will break as a result of volume expansion, thereby exposing the freshly deposited Li metal to the electrolyte, which in turn creates a new reaction interface. This repeated fracture and regeneration of the SEI film severely and irreversibly consumes the electrolyte and the Li metal, and lowers the coulombic efficiency during cycling. Simultaneously, this unstable electrolyte/electrode interface can lead to uneven Li metal deposition, which exacerbates the formation of Li dendrites [9]. Moreover, the uncontrolled Li dendrites may puncture the separator and cause an internal short-circuit. During the Li metal stripping process, a part of the isolated Li metal particles tends to strip from the root, which can cause them to detach from the conductive network to form “dead Li”. Dead Li can damage the evenness of the electrolyte/electrode interface, thereby creating a vicious cycle. Consequently, Li metal anodes are plagued by a short cycle lifespan and low coulombic efficiency [10].

Numerous effective strategies have been proposed to improve the cycling stability and safety performance of the Li metal anodes. These strategies can be mainly categorized into the following: functional electrolyte additives, artificial SEI films, and the modification of the conductive substrate. In a traditional electrolyte, an SEI film that is self-generated on the Li metal is usually uneven, lacks flexibility, and cannot relieve the volume change during the Li deposition procedure. Therefore, an ideal electrolyte/electrode interface should possess good flexibility to reduce the stress change, and enough mechanical strength to hinder the growth of Li dendrites. Therefore, functional electrolyte additives (fluoroethylene carbonate [11,12], vinylene carbonate [13], and vinyl ethylene carbonate [14]) are commonly used to improve the protective effect of an SEI film, and often play a key role in improving the cycling stability of Li metal anodes. However, the amount of electrolyte additives must be traced, which results in a relatively limited efficacy during prolonged cycling. Conversely, establishing an artificial SEI film requires the formation of a protective layer on the Li metal surface through a pretreatment procedure [15]. This pretreatment is generally chemical or physical and is often performed in a glove box. Although the protective layer formed in this process is highly controllable, the required experimental conditions are relatively harsh and difficult to apply to large scale production. In comparison, the preparation and modification of the conductive substrate can usually be completed in an air environment, and the operation method can be diversified. In addition, the conductive substrate can not only locally reduce current density, which accelerates uniform Li deposition, but also offer a host that can restrain Li dendrite growth. Therefore, layered reduced graphene oxide [16], nickel foam [17], copper foam [18], and vapor grown carbon fiber (VGCF) matrices have been proven to improve the stability of Li metal anodes, even at ultrahigh capacity and ultrahigh rate conditions [19]. Although a conductive substrate can enhance the cycle stability of Li metal batteries, most previous studies in this field are based on ether electrolytes [20–23]. The electrochemical performance of Li metal in ether electrolytes is better than that of commercial ester electrolytes; this is because, in the case of Li metal in ether electrolytes, a polymer film is formed on the surface of the metal. However, the voltage window of ether electrolytes is extremely low (less than 3.8 V compared to that of Li^+/Li), and is not compatible with widely used cathode materials, including $\text{LiNi}_x\text{Co}_y\text{Mn}_z\text{O}_2$, LiCoO_2 , and $\text{LiNi}_{0.8}\text{Co}_{0.15}\text{Al}_{0.05}\text{O}_2$, because they usually require a cut-off voltage of 4.3 V. Therefore, the modification of a conductive substrate based on a commercial carbonate-based electrolyte has a great potential for the practical application of Li metal batteries.

In our study, a realistic design of hydrogen titanate ($\text{H}_2\text{Ti}_3\text{O}_7$, HTO) nanowire arrays structure decorated with Ag nanoparticles (NPs) (Ag@HTO) was proposed as a dual-functional current collector to achieve a stable long lifespan with a highly reversible depo-

sition/stripping of Li metal in a carbonate-based electrolyte. As shown in Fig. 1(a), the combination of Ag NPs and the titanate arrays structure can be achieved via hydrothermal and silver mirror reactions. An advantage of the Ag@HTO structure is that it can perform a dual-functional role in Li deposition. On one hand, the HTO matrix homogenizes the Li ions to reduce concentration polarization. While, on the other hand, the addition of Ag NPs can effectively increase the electronic conductivity and provide stable nucleation sites, resulting in controllable Li deposition/stripping. Due to these advantages, an Ag@HTO current collector can effectively suppress the generation of Li dendrites and promote the uniform deposition of Li metal, which results in a stable and long-term lifecycle. In comparison, Li deposition on pristine Ti foil is quite irregular and uncontrollable (Fig. 1(c)).

2. Experimental

2.1. Preparation of HTO nanowire arrays on Ti substrate

Commercial Ti foil was first cut into a square block sample (5 cm in diameter, 50 μm in thickness) and washed ultrasonically in ethanol and acetone several times to remove impurities. Then, 1.4 g of NaOH was dissolved in 60 mL of deionized water. After ultrasonic dissolution for 30 min, 20 mL of ethanol was added to the compound solution. Next, the dry Ti foil and NaOH solution were transferred into a teflon-lined stainless steel autoclave. The prepared autoclave was heated to 210 $^\circ\text{C}$ at a rate of 3 $^\circ\text{C}/\text{min}$ for 3 h. After natural cooling to room temperature, the resultant synthesized precursor was washed several times. Then, the precursor was immersed in a 0.1 M of HCl (Xilong Chemical Company, China) solution for 6 h to exchange the Na^+ ions with H^+ ions, thereby facilitating the formation of HTO. After a deep wash with ethanol and deionized water, the preparation of the HTO nanowire arrays on the Ti substrate was conducted. The successful synthesis of HTO was suitably demonstrated when the surface of the Ti foil substrate was completely covered by light blue.

2.2. Preparation of Ag@HTO nanowire arrays

After the synthesis of HTO nanowire arrays on the Ti foil substrate, the HTO nanowire sample was dried for the preparation of Ag@HTO nanowire arrays via a typical silver mirror reaction. To start, the synthesized compound was placed in a 500 mL beaker, and 100 mL of the prepared AgNO_3 (Xilong Chemical Company, China) solution was added for 15 min. Next, the 0.1 mM NaOH solution was added dropwise to the beaker, causing a brown precipitate to form. The NaOH solution was continuously dropped until the color of solution no longer changed. Subsequently, a diluted ammonia solution (5 M) was added dropwise to the mixed solution until the brown precipitate completely disappeared and the solution became clear. Then, 0.18 g of glucose (Sinopharm Chemical Regent, China) was dissolved in 100 mL of deionized water before it was added in the mixed solution. After 3 h at room temperature, the Ag NPs were successfully supported on the HTO arrays substrate, and the surface of the experimental sample changed from bright blue to black. Finally, the Ag@HTO sample was dried at 60 $^\circ\text{C}$ and cut into the appropriate size of electrode for preparation of the anode current collector.

2.3. Characterization methods

To ensure the accuracy of measurement, the Li deposited current collector was cleaned several times by ethylene carbonate (EC) and dried at room temperature. Note that all operations occurred in an Ar filled atmosphere glove box. The morphology

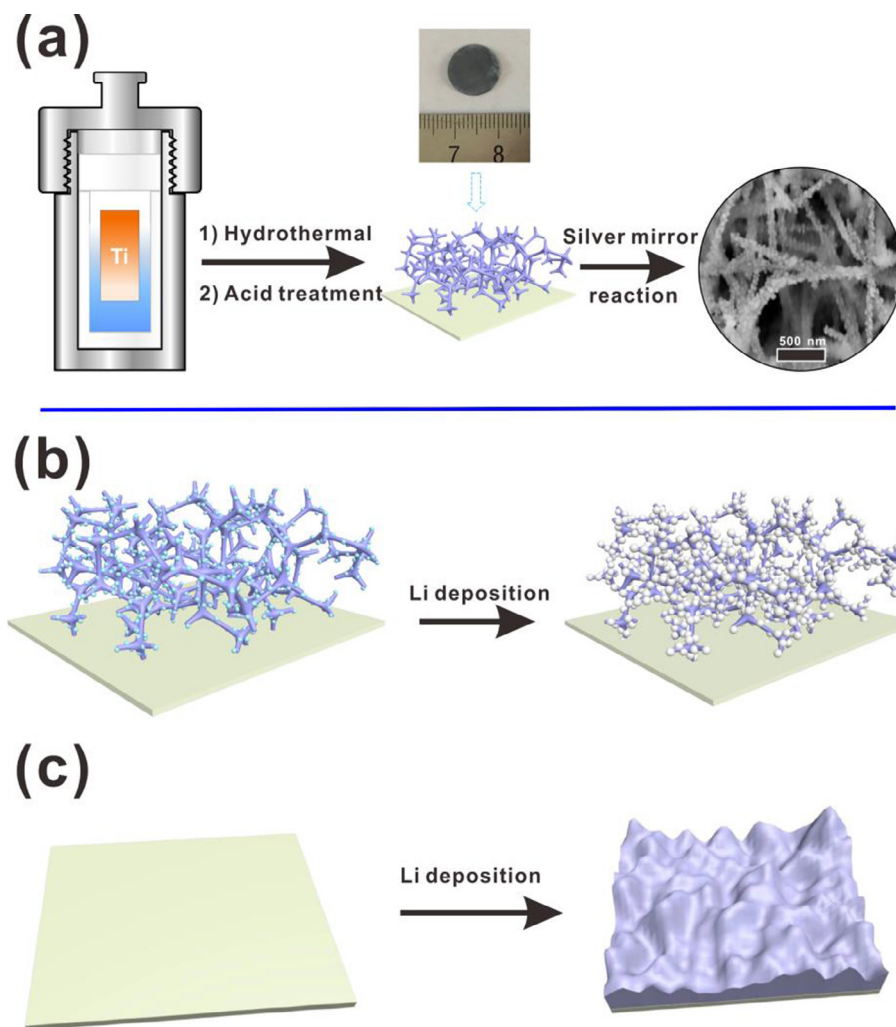


Fig. 1. (a) Illustration of the synthesis process of the Ag@HTO nanowire arrays current collector. (b) Schematic of Li deposition behavior on Ag@HTO nanowire arrays current collector and (c) pristine Ti foil current collector.

study was carried out using a scanning electron microscope (SEM, Hitachi 4800) and transmission electron microscope (TEM, Tecnai F30 TWIN). The X-ray diffraction (XRD, Rigaku MiniFlex/600) spectrum was collected with Cu $K\alpha$ radiation, and the electrolyte affinity property test was performed using a contact angle goniometer (Powereach JC2000C1, Shanghai Zhongchen Digital Technique Equipment Co., Ltd).

2.4. Electrochemical measurements

A CR2032 was used to test the coulombic efficiency, cycling impedance, and full cell properties for all the electrochemical measurements. Regarding the electrolyte, Li hexafluorophosphate (LiPF_6 , 1 M) was dissolved in an ethylene carbonate and dimethyl carbonate solution (1:1 in volume) with vinylene carbonate (VC, 5 wt%) for stable SEI formation.

To test the Li deposition efficiency, the pristine Ti foil and Ag@HTO sample were cut to size (12 mm in diameter) for use as working electrodes. Note that the pristine Ti foil was used as a reference electrode. During the half-cell assembly, 80 μL of the electrolyte was consumed. The half-cell was also applied to the Li coulombic efficiency and cycling impedance measurements where the deposition current density was controlled to 1 mAcm^{-2} and 2 mAcm^{-2} , and the deposition capacity was 1 mAh cm^{-2} . For the symmetric cell test, the pristine Ti foil and Ag@HTO sample were

initially deposited on 4 mAh cm^{-2} Li metal. Then, the Li deposited current collector was removed for pairing with another one to assemble a symmetry cell. The symmetry cell test was performed with a current density of 1 mA cm^{-2} and deposition capacity of 1 mAh cm^{-2} . The electrochemical impedance spectroscopy (EIS) was collected in the frequency range of 10 mHz – 100 kHz via an Autolab PGSTAT 101 cell test instrument.

To examine the full-cell properties, $\text{LiNi}_{0.5}\text{Co}_{0.2}\text{Mn}_{0.3}\text{O}_2$ (NCM523) was used as the cathode material. For preparation, NCM523, acetylene black, and poly(vinylidene fluoride) (PVDF) were mixed in N-methyl pyrrolidone (NMP) with a weight ratio of 8:1:1. After stirring overnight, the slurry was uniformly spread on aluminum foil, and dried at 80 $^\circ\text{C}$ overnight. The pristine Ti foil and HTO nanowire were predeposited at a capacity of 8 mAh cm^{-2} , which matches the NCM523 cathode's real mass loading of 3.0 mg cm^{-2} , to assemble full cells. One hundred μL of carbonate electrolyte was added to each cell. The test charging and discharging cut-off voltages were controlled to 4.3 V and 3.0 V, respectively.

3. Results and discussion

To understand the morphology and characteristic properties of Ag@HTO, SEM images of different magnification and their corresponding element mapping were obtained (Fig. 2). Ag metal pos-

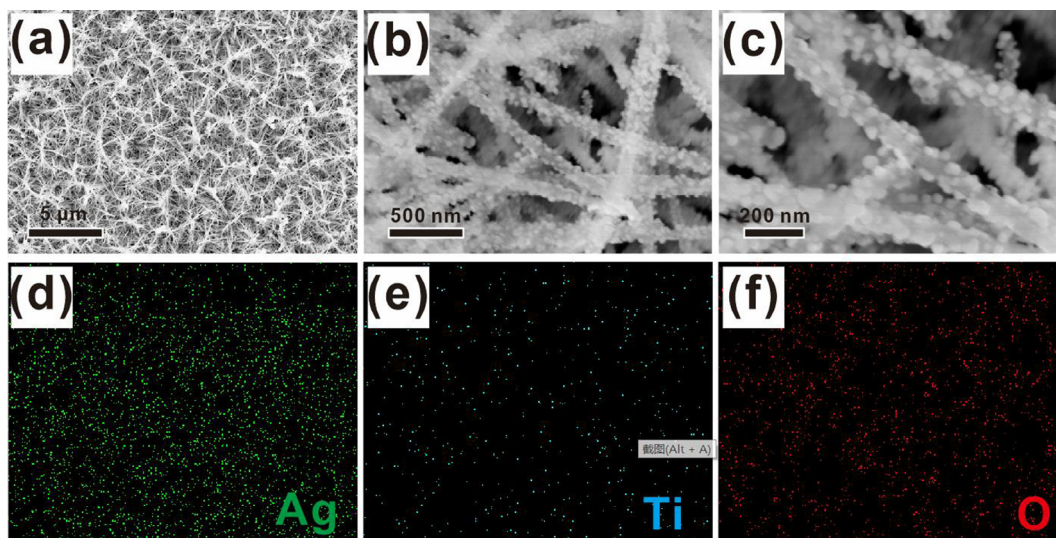


Fig. 2. (a, b, c) Different magnifications of the scanning electron microscope (SEM) images of the Ag@HTO current collector and the (d, e, f) corresponding element mapping.

sesses a high electrical conductivity (6.3×10^7 S/m) [24], and the uniform distribution of the Ag NPs help establish an excellent conductive network, which means that the Ti foil can form an equipotential body with the HTO array on its surface. Meanwhile, as seen in the corresponding element mapping of the Ag@HTO current collector (Fig. 2(d–f)), the Ag NPs are largely distributed in the HTO array current collector. Furthermore, it can be easily seen that the Ag@HTO current collector consists of abundant HTO nanowire arrays (Fig. 2(a)). As shown in Fig. S3 (Located in the Supporting Information), the thickness of the Ag@HTO nanowires on the Ti foil is 8.8 μm . These cross-linked HTO array structures effectively contribute to Li ion homogenization, which reduces the concentration polarization that occurs during the electrochemical reaction. The Ag@HTO nanowires, with widths ranging from approximately 80 nm to 100 nm, can be clearly seen in Fig. 2(b). Note that there are many pores between the Ag@HTO nanowires, which leaves a lot of space for Li metal deposition, thereby ensuring that more Li metal can be accommodated. From the higher magnification SEM images in Fig. 2(c), a large number of Ag NPs (20 nm) are distributed on the surface of the Ag@HTO nanowires. According to previous reports, Ag NPs have strong affinity with Li metal, which can greatly reduce the energy barrier for Li deposition [25,26]. Therefore, the Ag NPs on the surface of the HTO nanowire arrays are expected to improve the Li affinity of the entire Ag@HTO array current collector. With that in consideration, it may also be effective in preventing Li particles from detaching from the current collector during long-term cycling, which could reduce the generation of dead Li. Benefiting from the 3D cross-linked structure of the Ag@HTO arrays and the lithophilic property of Ag NPs, the array can achieve stable Li deposition [27–29].

To verify the composition and crystal morphology of Ag@HTO, the XRD pattern of Ag@HTO was evaluated, as shown in Fig. 3. As the HTO arrays were formed in-situ on Ti foil through a hydrothermal reaction, the large peaks of the Ti foil (marked with JCPDS No. 01-1198) are clearly observed [30]. After acid treatment, the diffraction peaks of layered HTO also appear in the XRD pattern at $2\theta = 24.3^\circ$, 29.0° , and 44.0° , which are in agreement with the experimental results of previous reports (marked with JCPDS No. 47-0124) [31,32]. After the silver mirror reaction, the cubic Ag phase diffraction peak appears clearly, indicating the successful loading of Ag NPs onto the HTO nanowire arrays. Based on these results, we successfully synthesized Ag NPs supported on HTO

nanowire arrays. Note that the subsequent alkaline silver mirror reaction did not affect the HTO structure.

In order to understand the distribution of Ag NPs on the surface of the HTO nanowire arrays and to verify the crystal structure of the Ag particles more accurately, the TEM and HRTEM images were evaluated, as seen in Fig. 3(b, c). Note that the diameter of the HTO nanowires is approximately 80 nm to 100 nm (Fig. 3(b)), which is in agreement with the previous observation from the direct SEM images. In addition, it can be seen that numerous Ag NPs with different diameters are scattered on the surface of the HTO nanowire arrays. The copious distribution of Ag NPs provides preferential nucleation sites during the initial stage of Li deposition, which helps Li metal to deposit uniformly within the HTO nanowire array. The spacing (0.24 nm) of the Ag NPs corresponds to the (111) crystal plane of the Ag NPs. The Fourier transform map of the Ag@HTO nanowire arrays HRTEM images clearly verify the structural state of the Ag NPs and HTO sample, where the observed crystal plane spacing correctly matches the crystal plane data of the HTO and Ag NPs, as shown in Fig. 3(c) [31,33]. Based on these results, the cubic Ag NPs were confirmed to have successfully synthesized through the silver mirror reaction, and as the result of the dispersion of the liquid reaction, the Ag NPs are well distributed on the surface of the HTO nanowire arrays, aiding the Li metal deposition process [34,35].

Coulombic efficiency is a critical parameter in the cell cycling process as it is used to evaluate the reversibility of the Li deposition/stripping process. During typical Li metal cycling, the amount of Li metal stripped is less than the amount deposited, as a result of the side reactions and generation of dead Li [36]. Note that the ratio of stripped to deposited Li is defined as the coulombic efficiency. The Ag@HTO was paired with Ti foil and assembled into a half-cell in order to explore the cycling stability during prolonged cycling. With the cycling conditions of 1 mA cm^{-2} and 1 mAh cm^{-2} , the coulombic efficiency of the pristine Ti foil and Ag@HTO current collector are shown in Fig. 4(a), wherein it is clear that the Ag@HTO can maintain a high coulombic efficiency (95.5%) during the initial 10 cycles, which is often difficult in a carbonate electrolyte. Since the stability of the SEI formed in the ester electrolyte is lower than that of the ether electrolyte, the reversibility of Li metal is usually poor. In contrast, the pristine Ti foil can only maintain a coulombic efficiency of 90% and 92% in the first 5 and 10 cycles, respectively. This indicates that the Ag@HTO current collec-

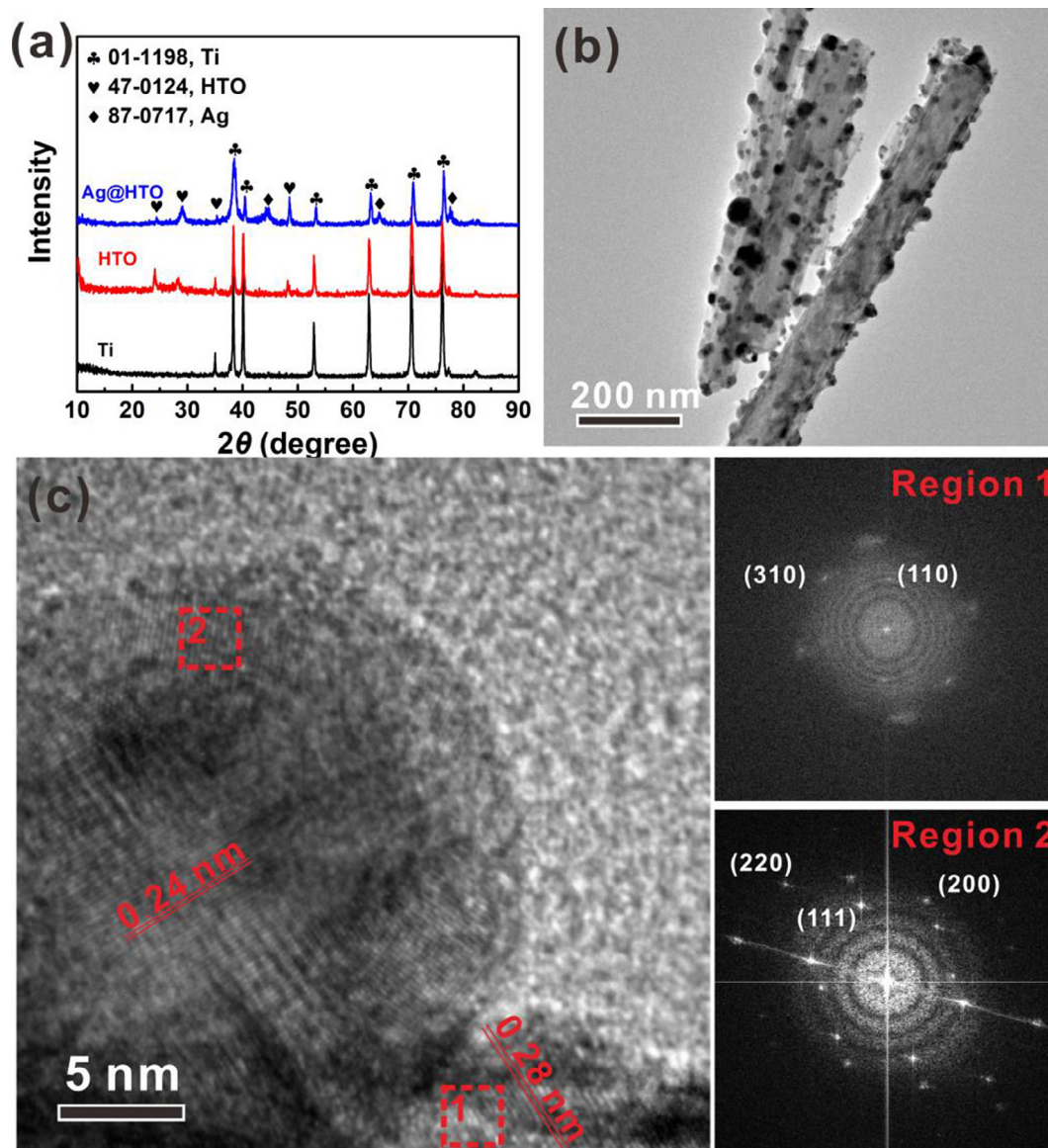


Fig. 3. (a) The X-ray diffraction (XRD) spectrum of different products during the synthesis of Ag@HTO nanowire arrays, (b) transmission electron microscope (TEM) images, (c) HRTEM image, and different region Fourier transform maps of Ag@HTO nanowire arrays.

tor can host the Li metal. After the subsequent 20 cycles, the coulombic efficiency of the pristine Ti foil exhibits a rapid decay and begins to fluctuate dramatically. This is because, after prolonged cycling, the surface of the Ti foil is covered with dead Li and a broken SEI, resulting in a low reversibility of Li metal. However, although the coulombic efficiency of the Ag@HTO current collector decreased slightly during cycling, it can still maintain stable cycle performance for up to 100 cycles. In previous studies, researchers found that the decrease in coulombic efficiency in traditional Li metal batteries is a result of the Li dendrites failing to participate in the reaction, thereby becoming dead Li. Therefore, we determined that the Ag@HTO current collector inhibits the generation of Li dendrites during cycling. The initial deposition process of Li metal includes both a nucleation and deposition process. Generally, the turning point in the voltage drop process is defined as the Li nucleation potential, which is a quantifiable parameter used to measure the affinity with Li. A higher nucleation potential means that it will create a more uneven deposition behavior [37,38]. Clearly, the affinity of Li and Ti foil is very poor. The Li nucleation potential (140 mV) has a negative impact on Li deposi-

tion behavior, which is shown in the initial deposition voltage curve of the pristine Ti foil (Fig. 4(b)). However, as there is good affinity between the Ag NPs and Li, the Ag NPs become nucleation sites for Li metal. Therefore, the entire initial deposition voltage of the Ag@HTO current collector is very smooth, and there is no obvious Li nucleation process. As the Ag@HTO current collector has a very low Li nucleation potential, Li is deposited evenly. During the long-cycle deposition of Li metal, the polarization voltage during Li deposition is another important parameter to evaluate the reversibility of Li metal. The Ag@HTO current collector is able to maintain a lower polarization voltage (13 mV) after 20 cycles and (15 mV) 40 cycles than the pristine Ti foil (32 mV), proving that it is more favorable for Li deposition (Fig. 4(c)). Nevertheless, the discharge voltage profiles tend to rise near the end of the 20 and 40 cycles for the pristine Ti foil electrode. This phenomenon is considered an “overpotential bump” at the end of the plating process, which can be explained by kinetic hindrance [39,40]. The poor lithiophilicity of the pristine Ti foil may result in the formation of an unstable SEI during the early cycles, possibly causing the kinetic hindrance at the end of the plating process of Li. In

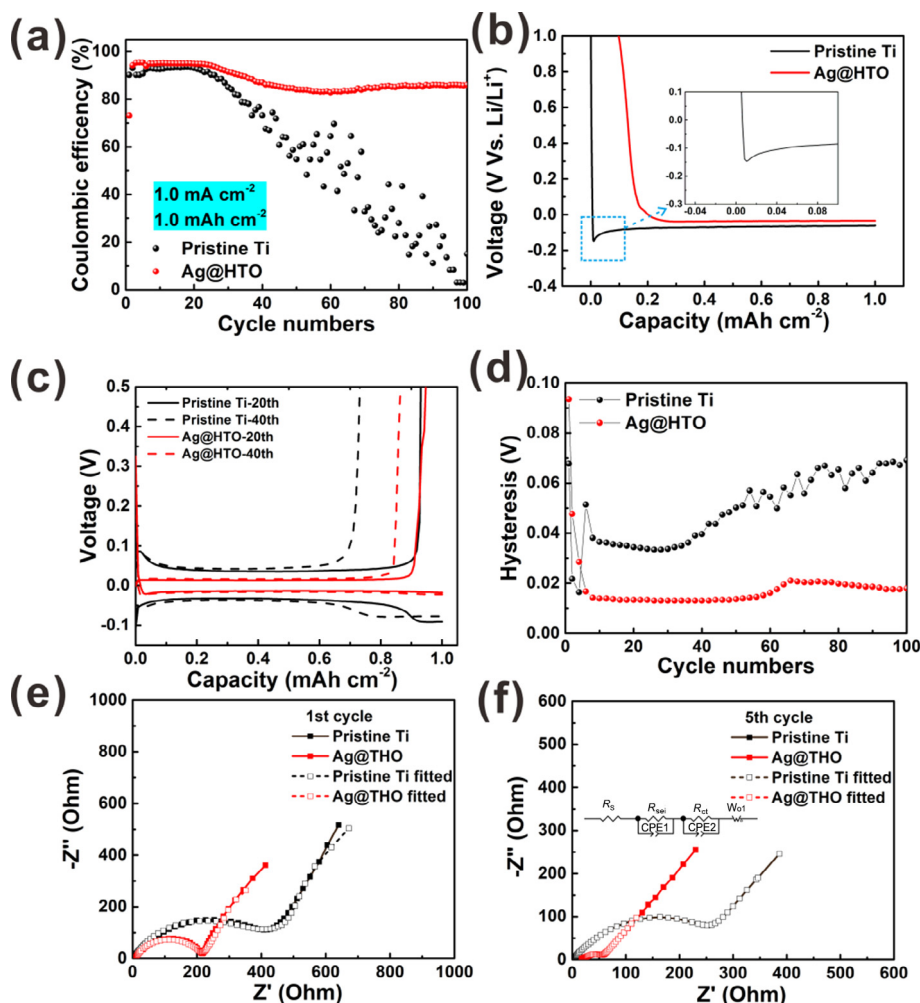


Fig. 4. Electrochemical performance of the pristine Ti foil and Ag@HTO nanowire arrays current collector. (a) The coulombic efficiency of pristine Ti foil and Ag@HTO at a current density of 1 mA cm^{-2} and capacity density of 1 mAh cm^{-2} . (b) Voltage profiles of pristine Ti foil and Ag@HTO at the first deposition process. (c) Comparison of voltage profiles of pristine Ti foil and Ag@HTO at 20 and 40 cycles. (d) The cycling hysteresis voltage of pristine Ti foil and Ag@HTO. (e, f) The EIS spectra of pristine Ti foil and Ag@HTO at 1 cycle and 5 cycles, respectively.

comparison, the overpotential bumps phenomenon does not occur in the Ag@HTO due to the good lithiophilicity of the Ag NPs, which contributes to the formation of a stable SEI [41]. After undergoing extensive cycling, the Ag@HTO current collector can maintain a stable Li deposition polarization voltage, which corresponds to its high Li deposition reversibility (Fig. 4(d)). In contrast, the pristine Ti foil maintains a relatively stable polarization voltage in the initial 30 cycles then increases rapidly, which is not conducive to uniform Li deposition. To further investigate the deposition process, the EIS spectra are shown in Fig. 4(e, f). Here, due to the different frequency corresponding to each interface, the impedance displayed by the first semicircle corresponds to an SEI film. After the initial formation of the SEI film, the R_{se} ($32.9 \ \Omega$) and R_{ct} ($194.8 \ \Omega$) of the Ag@HTO electrode are much smaller than that of the pristine Ti foil electrode, which are $116.1 \ \Omega$ and $335.8 \ \Omega$, respectively. During constant cycling, the Ag@HTO electrode exhibits a lower impedance (Table S1). Based on the results of the EIS spectra, the Ag@HTO current collector promotes the formation of an SEI layer by ensuring a lower impedance, which helps uniform Li metal deposition. In summary, the Ag@HTO current collector not only possesses a strong affinity with Li but can also promote a stable SEI layer. Therefore, it can achieve smooth and stable Li deposition and improve the cycle performance of Li metal batteries.

To understand the Li dendrite formation inhibited by the Ag@HTO nanowire arrays, the morphology of the deposition is illustrated in Fig. 5. Clearly, the growth of Li metal is dendritic in the pristine Ti foil owing to the weak affinity between Ti and Li. The Li dendrites not only accelerate the consumption of Li metal but also lead to safety risks. In comparison, the Li metal can uniformly deposit on the Ag@HTO nanowire arrays owing to the strong affinity between Ag and Li, which can be confirmed from Fig. S2. Therefore, the Ag@HTO current collector can act as a host for the Li metal, thereby ensuring that it does not grow indefinitely. After 10 cycles, needle-like Li can be observed in the pristine Ti foil (Fig. 5(c)), which is caused by the unlimited expansion of the Li metal. No obvious Li dendrites occur in the Ag@HTO current collector, and the Li metal is also deposited inside the array structure, which effectively relieves the volume expansion of the metal (Fig. 5(d)). Furthermore, the contact angle test results show that Ag@HTO can maintain better affinity with the electrolyte than the pristine Ti foil, further strengthening the Li ion homogenization (Fig. 5(e, f)). The Ag@HTO current collector can restrain Li dendrites and alleviate the volume expansion of Li metal during the charge/discharge process; therefore, it can promote the realization of uniform Li deposition behavior.

In order to further verify the superiority of the Ag@HTO current collector compared with the pristine Ti on Li metal-based batteries,

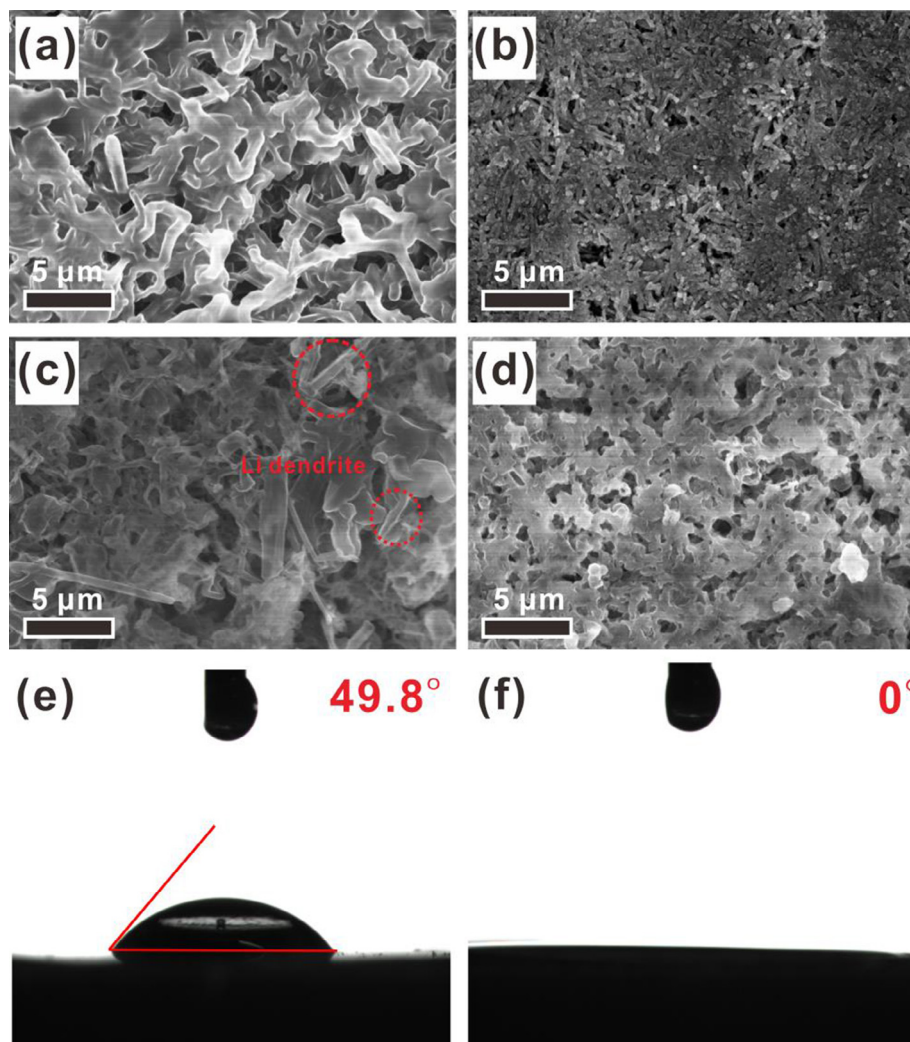


Fig. 5. Li deposition SEM images of the (a, c) pristine Ti foil with deposition capacity of 4 mAh cm^{-2} and (b, d) Ag@HTO after 1 cycle and 10 cycles. (e, f) The contact angle test results of the pristine Ti foil and Ag@HTO.

a full cell was selected to measure the performance differences. As the ester electrolyte can withstand a higher voltage, the high energy density NCM523 was selected as the cathode material. In separate tests, the pristine Ti and Ag@HTO current collectors with 8 mAh cm^{-2} Li predeposited were used as negative electrodes. Note that when combined with the mass loading of Ag@HTO ($0.3625 \text{ mg cm}^{-1}$), the specific capacity of the composite anode is calculated to be $3285.4 \text{ mAh g}^{-1}$. The cycling performance of the full cells at 1 C, which is calculated based on the mass of the cathode electrode, with the pristine Ti foil (Ti||NCM) and Ag@HTO current collector (Ag||NCM) are shown in Fig. 6(a). The initial discharge capacity of the two cells is close, and the coulombic efficiency reaches nearly 100% in the initial 50 cycles. However, as the cycles continue, the capacity of Ti||NCM begins to decrease sharply, and the coulombic efficiency was only approximately 90%, which means that only 10% of the Li metal is lost in each cycle. After 100 cycles, the cell capacity of Ti||NCM decreases to 0. In contrast, the Ag||NCM could maintain a coulombic efficiency of 99.5% during prolonged cycling, along with a high capacity retention of 81.2%, even after 200 cycles. The galvanostatic charge/discharge curves of the Ti||NCM and Ag||NCM at 1 C are illustrated in Fig. 6(b, c). The Ag||NCM maintains a typical NCM523 electrode charge/discharge curve during 200 cycles while the Ti||NCM clearly has a higher polarization voltage, and the discharge platform is not

easily identified. Moreover, the excellent performance of Ag||NCM is reflected at a rate of 2 C, as shown in Fig. 6(d), where the Ag||NCM maintains a high capacity retention ratio of 89.2% even after 120 cycles, which the Ti||NCM failed to do so after only 70 cycles. Furthermore, the Ag||NCM exhibited outstanding superiority in high-rate cycling (Fig. 6(e)). Note that at the high rates of 5 C and 10 C, Ag||NCM can exhibit capacities of 133 mAh g^{-1} and 114 mAh g^{-1} , respectively. Therefore, due to the dual-function of the Ag@HTO current collector in a Li metal anode, it can simultaneously achieve a high coulombic efficiency and a long lifespan, while displaying superiority in high rate tests.

4. Conclusions

In this study, HTO nanowire arrays decorated with homogenous Ag NPs were successfully synthesized via simple hydrothermal and silver mirror reactions. The characteristic results show that the Ag@HTO exhibits a 3D cross-linked array structure where Ag NPs are evenly distributed on the surface of HTO. When applied in a full cell with a NCM523 cathode material, the Ag||NCM could maintain a capacity retention ratio of 81.2% at a rate of 1 C after 200 cycles, while the pristine Ti failed to do so after only 70 cycles. Additionally, the Ag||NCM showed superiority in terms of cycling perfor-

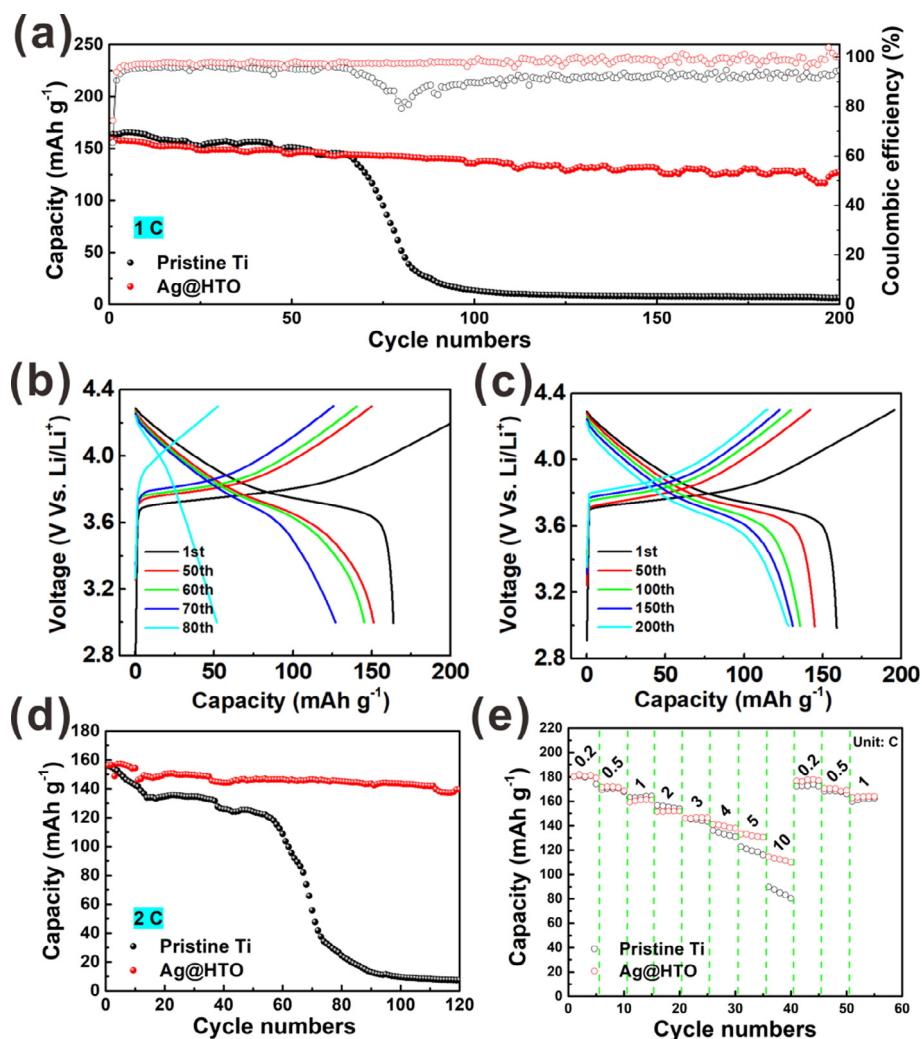


Fig. 6. The full-cell electrochemical performance with NCM523 cathode material in a carbonate-based electrolyte. (a) The long time cycling performance of the pristine Ti foil (Ti||NCM) and Ag@HTO current collectors (Ag||NCM) at a rate of 1 capacity (C). (b) The voltage profiles of Ti||NCM and (c) Ag||NCM at the rate of 1 C at different cycles. (d) The cycling performances of Ti||NCM and Ag||NCM at rate of 2 C. (e) The comparison in cycling performance of Ti||NCM and Ag||NCM at different rates.

mance during different rate tests. These improvements were a result of the structure of Ag@HTO, which offers a dual-functional role in Li deposition. The HTO matrix homogenizes the Li ions to reduce the concentration polarization, while the addition of Ag NPs effectively increases the electronic conductivity and provides stable nucleation sites, thereby resulting in a controlled Li deposition/stripping. This study reveals a new method for designing current collectors paired with high voltage cathodes for creating high energy density Li metal batteries.

Declaration of Competing Interest

The authors declare that they have no known competing financial interests or personal relationships that could have appeared to influence the work reported in this paper.

Acknowledgments

This work is supported by the National Natural Science Foundation of China (Nos. 2127318, 21621091, and 21875195), the National Key Research and Development Program of China (No. 2017YFB0102000), and the Fundamental Research Funds for the Central Universities (No. 20720190040).

Appendix A. Supplementary data

Supplementary data to this article can be found online at <https://doi.org/10.1016/j.jechem.2020.05.057>.

References

- [1] B. Dunn, H. Kamath, J.M. Tarascon, *Science* 334 (2011) 928–935.
- [2] Y. Yang, H. Zhu, J.F. Xiao, H.B. Geng, Y.F. Zhang, J.B. Zhao, G. Li, X.L. Wang, C.C. Li, Q. Liu, *Adv. Mater.* 32 (2020) 1905295.
- [3] X.B. Cheng, R. Zhang, C.Z. Zhao, Q. Zhang, *Chem. Rev.* 117 (2017) 10403–10473.
- [4] H. Liu, X.B. Cheng, Z.H. Jin, R. Zhang, G.X. Wang, L.Q. Chen, Q.B. Liu, J.Q. Huang, Q. Zhang, *EnergyChem.* 1 (2019) 100003.
- [5] X.Q. Zhang, X.B. Cheng, Q. Zhang, *Adv. Mater Interfaces.* 5 (2018) 1701097.
- [6] H.J. Yang, C. Guo, A. Naveed, J.Y. Lei, J. Yang, Y.N. Nuli, J.L. Wang, *Energy Storage Mater.* 14 (2018) 199–221.
- [7] Y. Lu, Z. Tu, L.A. Archer, *Nat. Mater.* 13 (2014) 961–969.
- [8] J. Betz, J.P. Brinkmann, R. Nölle, C. Lürenbaum, M. Kolek, M.C. Stan, M. Winter, T. Placke, *Adv. Energy Mater.* 9 (2019) 1900574.
- [9] D. Wang, C. Qin, X. Li, G. Song, Y. Liu, M. Cao, L. Huang, Y. Wu, *iScience.* 23 (2020) 100781.
- [10] L. Wang, Z.Y. Zhou, X. Yan, F. Hou, L. Wen, W.B. Luo, J. Liang, S.X. Dou, *Energy Storage Mater.* 14 (2018) 22–48.
- [11] E. Markevich, G. Salitra, D. Aurbach, *ACS Energy Lett.* 2 (2017) 1337–1345.
- [12] E. Markevich, G. Salitra, F. Chesneau, M. Schmidt, D. Aurbach, *ACS Energy Lett.* 2 (2017) 1321–1326.
- [13] H. Ota, K. Shima, M. Ue, J. Yamaki, *Electrochim Acta* 49 (2004) 565–572.
- [14] Y. Yang, J. Xiong, S.B. Lai, R. Zhou, M. Zhao, H.B. Geng, Y.F. Zhang, Y.X. Fang, C.C. Li, J.B. Zhao, *ACS Appl Mater Inter.* 11 (2019) 6118–6125.

- [15] Y. Gu, W.W. Wang, Y.J. Li, Q.H. Wu, S. Tang, J.W. Yan, M.S. Zheng, D.Y. Wu, C.H. Fan, W.Q. Hu, Z.B. Chen, Y. Fang, Q.H. Zhang, Q.F. Dong, B.W. Mao, *Nat. Commun.* 9 (2018) 1339.
- [16] D. Lin, Y. Liu, Z. Liang, H.W. Lee, J. Sun, H. Wang, K. Yan, J. Xie, Y. Cui, *Nat. Nanotechnol.* 11 (2016) 626–632.
- [17] Z.P. Wen, Y.Y. Peng, J.L. Cong, H.M. Hua, Y.X. Lin, J. Xiong, J. Zeng, J.B. Zhao, *Nano Res.* (2019) 1–9.
- [18] Y.L. An, H.F. Fei, G.F. Zeng, X.Y. Xu, L.J. Ci, B.J. Xi, S.L. Xiong, J.K. Feng, Y.T. Qian, *Nano Energy.* 47 (2018) 503–511.
- [19] Y. Yang, J. F. Xiao, C. Y. Liu, D. J. Chen, H. B. Geng, Y. F. Zhang, J. B. Zhao, C. C. Li, W. D. He, *iScience.* (2020)
- [20] Q. Li, S.P. Zhu, Y.Y. Lu, *Adv. Funct. Mater.* 27 (2017) 1606422.
- [21] C. Zhao, C. Yu, S. Li, W. Guo, Y. Zhao, Q. Dong, X. Lin, Z. Song, X. Tan, C. Wang, M. Zheng, X. Sun, J. Qiu, *Small* 14 (2018) 1803310.
- [22] X. Ke, Y.H. Liang, L.H. Ou, H.D. Liu, Y.M. Chen, W.L. Wu, Y.F. Cheng, Z.P. Guo, Y. Q. Lai, P. Liu, Z.C. Shi, *Energy Storage Mater.* 23 (2019) 547–555.
- [23] L. Fan, H.L. Zhuang, W.D. Zhang, Y. Fu, Z.H. Liao, Y.Y. Lu, *Adv. Energy Mater.* 8 (2018) 1703360.
- [24] Z.P. Wen, Y.X. Lin, Y.Y. Peng, J. Zeng, J.B. Zhao, *J. Electrochem Soc.* 167 (2020) 020532.
- [25] K. Yan, Z.D. Lu, H.W. Lee, F. Xiong, P.C. Hsu, Y.Z. Li, J. Zhao, S. Chu, Y. Cui, *Nat. Energy.* 1 (2016) 16010.
- [26] X. Chen, X.R. Chen, T.Z. Hou, B.Q. Li, X.B. Cheng, R. Zhang, Q. Zhang, *Sci Adv.* 5 (2019).
- [27] P. Shi, T. Li, R. Zhang, X. Shen, X.B. Cheng, R. Xu, J.Q. Huang, X.R. Chen, H. Liu, Q. Zhang, *Adv. Mater.* 31 (2019) e1807131.
- [28] P. Shi, X.Q. Zhang, X. Shen, R. Zhang, H. Liu, Q. Zhang, *Adv. Mater Technol.* 5 (2019).
- [29] C. Niu, H. Pan, W. Xu, J. Xiao, J.G. Zhang, L. Luo, C. Wang, D. Mei, J. Meng, X. Wang, Z. Liu, L. Mai, J. Liu, *Nat. Nanotechnol.* 14 (2019) 594–601.
- [30] H.C. Lin, X. Li, X.Y. He, J.B. Zhao, *Electrochim Acta* 173 (2015) 242–251.
- [31] L.F. Que, F.D. Yu, L.L. Zheng, Z.B. Wang, D.M. Gu, *Nano Energy* 45 (2018) 337–345.
- [32] M. Shirpour, J. Cabana, M. Doeff, *Energy Environ. Sci.* 6 (2013) 2538–2547.
- [33] L.F. Que, Z.B. Wang, F.D. Yu, D.M. Gu, *J. Mater. Chem. A.* 4 (2016) 8716–8723.
- [34] X.R. Chen, B.Q. Li, C. Zhu, R. Zhang, X.B. Cheng, J.Q. Huang, Q. Zhang, *Adv. Energy Mater.* 9 (2019).
- [35] Y. Zhang, C.W. Wang, G. Pastel, Y.D. Kuang, H. Xie, Y.J. Li, B.Y. Liu, W. Luo, C.J. Chen, L.B. Hu, *Adv. Energy Mater.* 8 (2018).
- [36] C. Fang, J. Li, M. Zhang, Y. Zhang, F. Yang, J.Z. Lee, M.H. Lee, J. Alvarado, M.A. Schroeder, Y. Yang, B. Lu, N. Williams, M. Ceja, L. Yang, M. Cai, J. Gu, K. Xu, X. Wang, Y.S. Meng, *Nature* 572 (2019) 511–515.
- [37] H. Duan, J. Zhang, X. Chen, X.D. Zhang, J.Y. Li, L.B. Huang, X. Zhang, J.L. Shi, Y.X. Yin, Q. Zhang, Y.G. Guo, L. Jiang, L.J. Wan, *J. Am. Chem. Soc.* 140 (2018) 18051–18057.
- [38] R. Zhang, X.R. Chen, X. Chen, X.B. Cheng, X.Q. Zhang, C. Yan, Q. Zhang, *Angew. Chem. Int. Ed. Engl.* 56 (2017) 7764–7768.
- [39] J. Heine, S. Krüger, C. Hartnig, U. Wietelmann, M. Winter, P. Bieker, *Adv. Energy Mater.* 4 (2014).
- [40] Y. Liu, D. Lin, Z. Liang, J. Zhao, K. Yan, Y. Cui, *Nat. Commun.* 7 (2016) 10992.
- [41] G. Bieker, M. Winter, P. Bieker, *Phys. Chem. Chem. Phys.* 17 (2015) 8670–8679.